Since January 2020 Elsevier has created a COVID-19 resource centre with free information in English and Mandarin on the novel coronavirus COVID-19. The COVID-19 resource centre is hosted on Elsevier Connect, the company's public news and information website.

Journal of Saudi Chemical Society (2022) **26**, 101453

King Saud University

Journal of Saudi Chemical Society

www.ksu.edu.sa
www.sciencedirect.com

ORIGINAL ARTICLE

In silico exploration of binding potentials of anti SARS-CoV-1 phytochemicals against main protease of SARS-CoV-2

Abdullah G. Al-Sehemi [a,b], Mehboobali Pannipara [a,b,*], Rishikesh S. Parulekar [c], Jaydeo T. Kilbile [d], Prafulla B. Choudhari [c], Mubarak H. Shaikh [e]

[a] *Research Center for Advanced Materials Science, King Khalid University, Abha, Saudi Arabia*
[b] *Department of Chemistry, King Khalid University, Abha, Saudi Arabia*
[c] *Department of Pharmaceutical Chemistry, Bharati Vidyapeeth College of Pharmacy, Kolhapur 416 013, India*
[d] *Department of Basic and Applied Sciences, MGM University, Aurangabad 431 001, India*
[e] *Departrment of Chemistry, Radhabai Kale Mahila Mahavidyalaya, Ahmednagar 414 001 India*

Received 25 January 2022; revised 5 March 2022; accepted 6 March 2022
Available online 11 March 2022

KEYWORDS

SARS-CoV-1;
Phytochemicals;
SARS-CoV-2;
Main protease;
Molecular docking;
Molecular dynamics (MD) simulation

Abstract The phytochemicals can play complementary medicine compared to synthetic drugs considering their natural origin, safety, and low cost. Phytochemicals hold a key position for the expansion of drug development against corona viruses and need better consideration to the agents that have already been shown to display effective activity against various strains of corona viruses. In this study, we performed molecular docking studies on potential forty seven phytochemicals which are SARS-CoV-1 M^{pro} inhibitors to identify potential candidate against the main proteins of SARS-CoV-2. *In Silico* Molecular docking studies revealed that phytochemicals **16** (Broussoflavan A), **22** (Dieckol), **31** (Hygromycin B), **45** (Sinigrin) and **46** (Theaflavin-3,3′-digallate) exhibited excellent SARS-CoV-2 M^{pro} inhibitors. Furthermore, supported by Molecular dynamics (MD) simulation analysis such as Root Mean Square Deviation (RMSD), Root Mean Square Fluctuation (RMSF), Radius of gyration (Rg) and H-bond interaction analysis. We expect that our findings will provide designing principles for new corona virus strains and establish important frameworks for the future development of antiviral drugs.

* Corresponding author at: Department of Chemistry, King Khalid University, Abha, Saudi Arabia.
E-mail address: mpannipara@kku.edu.sa (M. Pannipara).
Peer review under responsibility of King Saud University.

Production and hosting by Elsevier

1. Introduction

Current high outline, global outbreaks of viral diseases from the coronavirus family have been caused by enveloped viruses. Acute respiratory tract inflammation caused by SARS-CoV-2 is an infectious disease, often fatal, that is characterized by the rapid and unexpected spread. Worldwide, the COVID-19

https://doi.org/10.1016/j.jscs.2022.101453

pandemic has recorded, as of 1st March 2022, 437 million cases, 369 million recovered cases with 5.97 million deaths, and the numbers continue to increase progressively [1] (https://covid19.who.int/). Furthermore, patients with pre-existing kidney dysfunction, immune-compromised persons, pulmonary disease and diabetes are the most susceptible community with higher mortality rates from SARS-CoV-2 infection. Coronavirus families are able to cause a number of diseases, such as hepatitis, gastroenteritis, bronchitis, systemic diseases, and even death in birds, humans, and other animals [2]. The contagion effect of such epidemic could possibly bring key challenges to worldwide health systems and have far-reaching significances on the global economy if it is not controlled effectively.

The SARS coronavirus is the viable microorganism accountable for the worldwide outburst of a severe disease that caused several deaths [3]. To design the anti-SARS drug, the coronavirus main protease (M^{pro}), recognized as the utmost attractive target due to its crucial role in facilitating viral transcription and replication [4]. Near about 30,000 nucleotides comprised in the SARS-CoV-2 genome: the gene of SARS-CoV-2 namely, replicase encodes pp1a and pp1ab two overlapping polyproteins which are essential for viral replication and transcription [5]. Polyproteins excreted the functional polypeptides by extensive proteolytic processing, mostly by the 33.8-kDa M^{pro} (also known as 3C-like protease). Polyprotein digested by M^{pro} at least 11 conserved sites, initially the autolytic cleavage of this enzyme itself from pp1a and pp1ab [6]. In the viral life cycle M^{pro} plays functional importance, shared with the absence of closely associated homologues in humans, recognize M^{pro} as an attractive target for the design of antiviral drugs [7].

Herein we describe the *in silico* molecular docking results that intended quickly discovery of lead compounds for clinical use, by assimilation structure-assisted drug design, virtual drug screening. This *in silico* study focused on identifying drug leads that target main protease (M^{pro}) of SARS-CoV-2. Jin and co-worker identified a mechanism-based inhibitor by computer-aided drug design, and then determined the crystal structure of M^{pro} of SARS-CoV-2 [8]. We have screened 47 SARS-CoV-1 M^{pro} active phytochemicals for high binding affinity and interaction to the conserved residues of the substrate-binding pocket of SARS-CoV-2 M^{pro} using molecular docking-based virtual screening. Our results demonstrated the efficacy of our screening strategy, which can lead to the rapid discovery of drug leads with clinical potential in response to new infectious diseases for which no specific drugs or vaccines are available.

2. Results and discussion

2.1. Molecular docking analysis

Molecular docking study was performed to explore the binding potential of the selected phytochemicals against the M^{pro} of SARS-CoV-2. Structure of the M^{pro} of SARS-CoV-2 (PDB ID: 6W63) [9] was downloaded from the free protein database www.rcsb.org.

The phytochemical analyzed in this work are showed profound activity against SARS-CoV-1 and their possible mode of action is via inhibition of the main protease. SARS-CoV-2 is mutated form of the main protease of SARS-CoV-1 and has up to 96% similarity [10,11]. Table 1 shows structures of phytochemicals utilized in current study. In virtue of all these reports, we thought virtual analysis of the molecules with profound activity on the SARS-CoV-1 on main protease of SARS-CoV-2 will be an attractive strategy for identification and development of potent inhibitors against viruses. Thus, phytochemicals with reported activity against SARS-CoV-1 were selected for the docking analysis [12–14].Grip based docking simulation was performed and best molecules were analyzed on the basis of docking score and binding interactions with M^{pro} of SARS-CoV-2.

Broussoflavan A (**16**) was found to be most active in docking simulation with showing docking score of −91.22 and hydrogen bond interaction with SER144(1.5 Å), CYS145 (1.6 Å) and CYS166(2.5 Å), aromatic interaction with HIS41 (1.5 Å) and hydrophobic interaction with HIS41, PHE140, LEU141, ASN142, SER144, CYS145, MET165, GLU166, LEU167, PRO168 as shown in Fig. 1.

Theaflavin-3,30-digallate (**46**) was found to be another active molecule in docking simulation with showing docking score of −76.85 and hydrogen bond interaction with THR26 (1.6 Å), CYS44(2.3 Å), CYS145(2.1 Å) HIS164(2.0 Å), MET165(2.0 Å), GLU166(2.5 Å), ARG188(1.8 Å), aromatic interaction with HIS41(4.6 Å) and hydrophobic interaction with HIS41, HIS 46 as shown in Fig. 2.

Dieckol (**22**) was found to be showing docking score of −73.11 and hydrogen bond interaction with TYR54(2.3 Å), SER139(2.4 Å), GLU166(2.2 Å), ARG188(2.5 Å) aromatic interaction with HIS41(4.4 Å) as shown in Fig. 3.

4′-O-Methyldiplacol (**4**) was found to be another phytochemical active in docking simulation with showing docking score of −68.78 and hydrogen bond interaction with HIS163 (2.5 Å), aromatic interaction with HIS41(5.0 Å) and hydrophobic interaction with HIS41, ASN142, MET165, GLU166 as shown in Fig. 4.

Sinigrin (**45**) showing docking score of −65.08 and hydrogen bond interactions with CYS145(2.5 Å), GLU166(2.2 Å), THR190(2.5 Å), GLN192(2.6 Å) and hydrophobic interaction with MET165, GLU166, PRO168, GLN189, as shown in Fig. 5.

Hygromycin B (**31**) showing docking score of −62.48 and hydrogen bond interactions with HIS41(2.0 Å), TYR54 (2.2 Å), PHE140(2.5 Å), SER144(2.0 Å), CYS145(1.5 Å), GLU166(2.2 Å) GLN189(2.5 Å), charge interaction with GLU166(2.4 Å) and hydrophobic interaction with THR25, HIS41, CYS44, THR45, MET49, PHE140, LEU141, ASN142, SER144, CYS145, MET165, GLU166, ARG188, GLN189 as shown in Fig. 6.

4′-O-Methyldiplacone (**5**) showing docking score of −60.58 and hydrogen bond interactions with ASN142(2.5 Å), aromatic interaction with HIS41(5.2 Å) and hydrophobic interaction with THR25, HIS41, ASN142, MET165, GLU166 as shown in Fig. 7.

2.2. Molecular dynamics (MD) simulation analysis

The molecular docking study revealed the most promising phytochemical inhibitor molecules against SARS-CoV-2 M^{pro} protein and so these docked complexes were selected for simulations. MD simulations were performed with control

Table 1 The chemical structures of known phytochemical compounds acting against SARS-CoV-1.

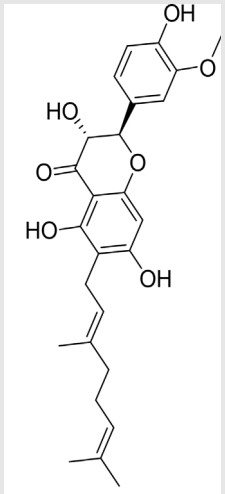

1

3'-O-Methyldiplacol

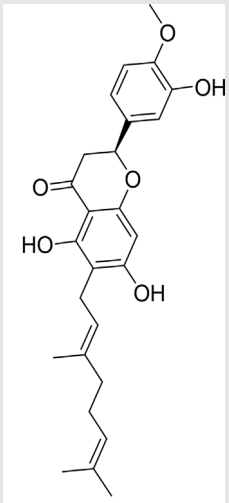

2

3'-O-methyldiplacone

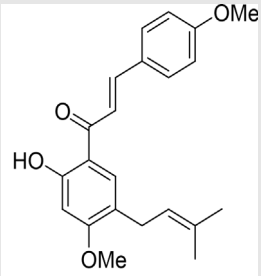

3

4'-O-methylbavachalcone

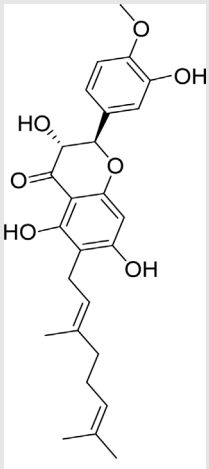

4

4'-O-Methyldiplacol

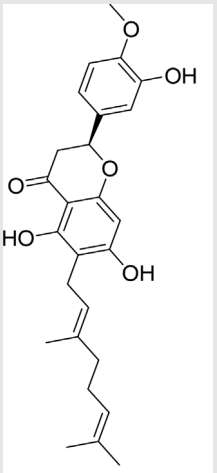

5

4'-O-Methyldiplacone

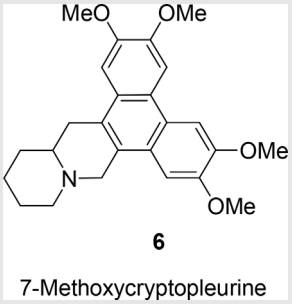

6

7-Methoxycryptopleurine

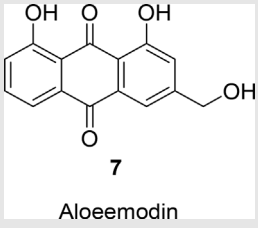

7

Aloeemodin

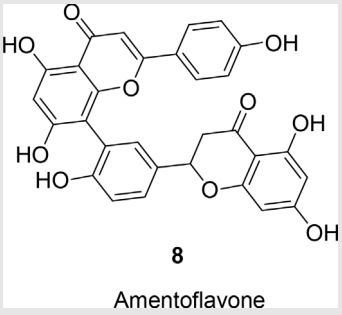

8

Amentoflavone

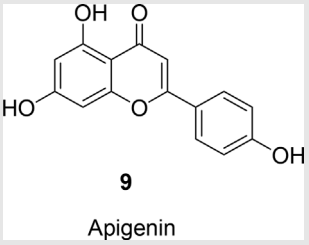

9

Apigenin

(*continued on next page*)

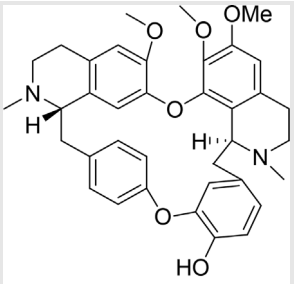

10

Berbamine

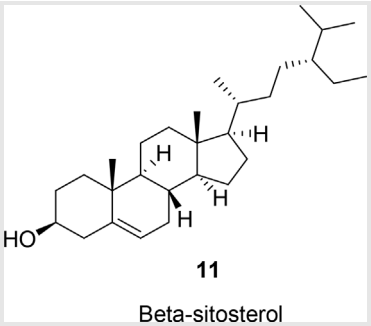

11

Beta-sitosterol

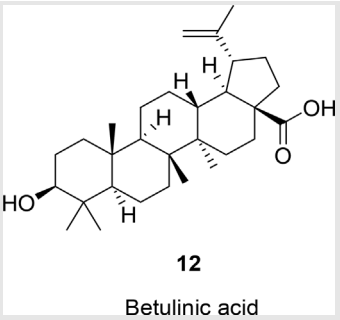

12

Betulinic acid

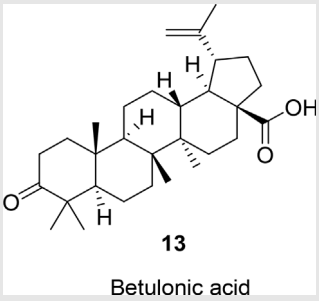

13

Betulonic acid

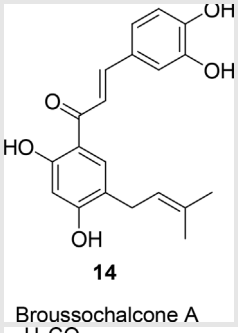

14

Broussochalcone A

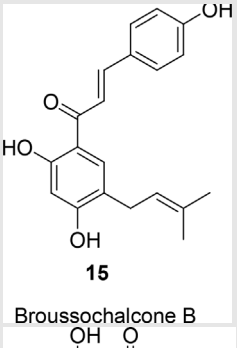

15

Broussochalcone B

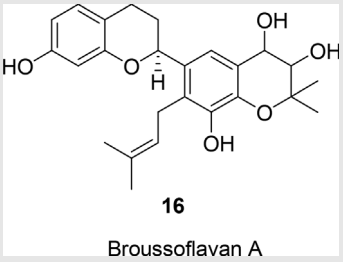

16

Broussoflavan A

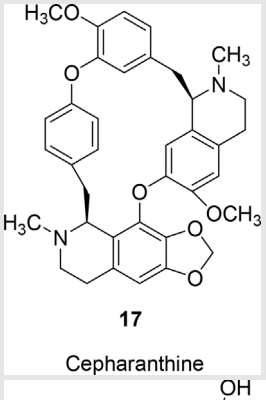

17

Cepharanthine

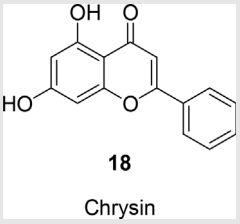

18

Chrysin

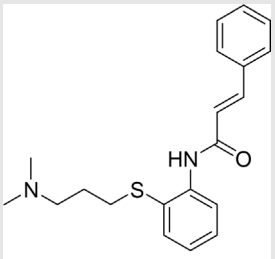

19

Cinanserin

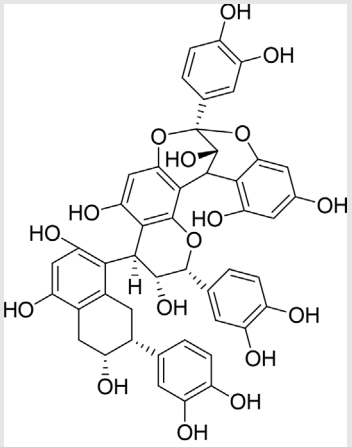

20

Cinnamtannin B1

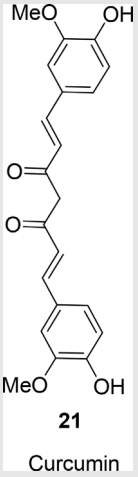

21

Curcumin

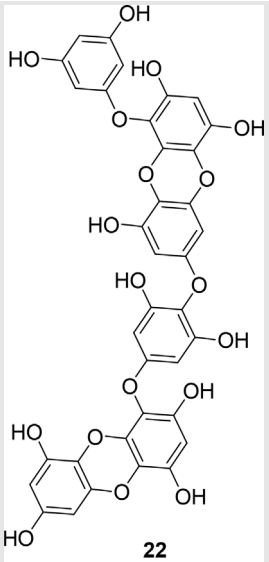

22

Dieckol

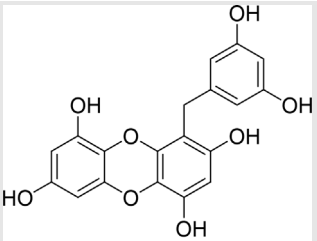

23

Eckol

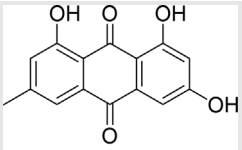

24

Emodin

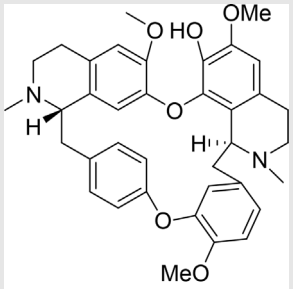

25

Fangchinoline

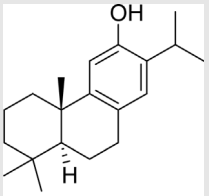

26

Ferruginol

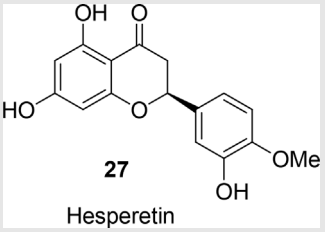

27

Hesperetin

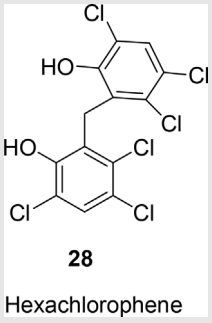

28

Hexachlorophene

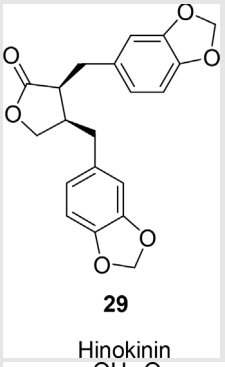

29

Hinokinin

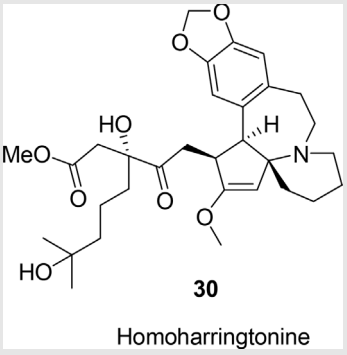

30

Homoharringtonine

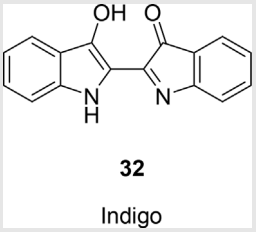

32

Indigo

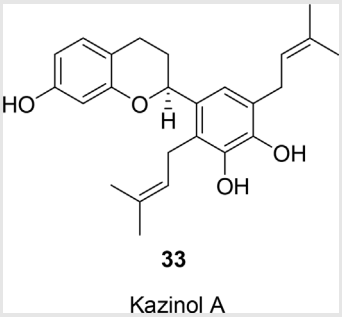

33

Kazinol A

(*continued on next page*)

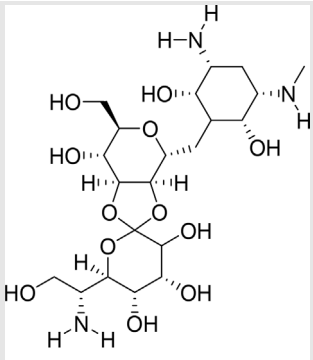

31

Hygromycin B

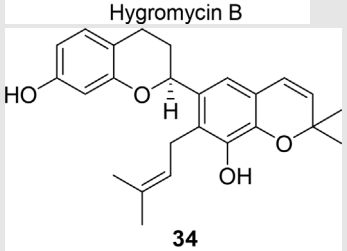

34

Kazinol B

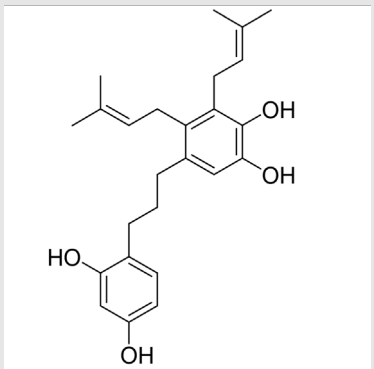

35

Kazinol F

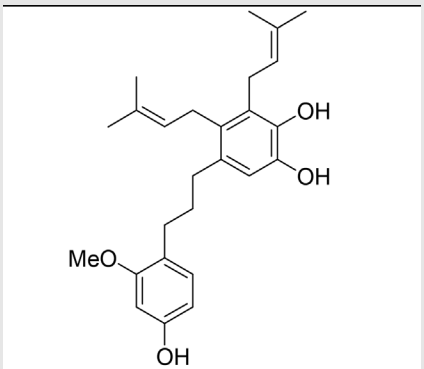

36

Kazinol J

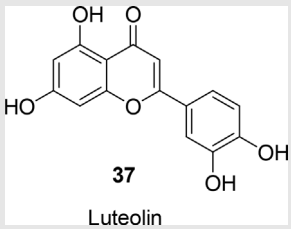

37

Luteolin

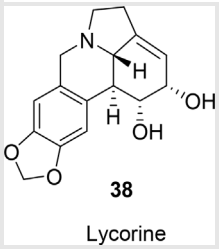

38

Lycorine

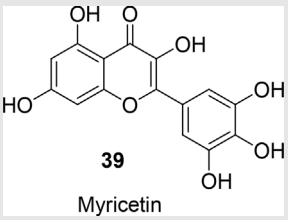

39

Myricetin

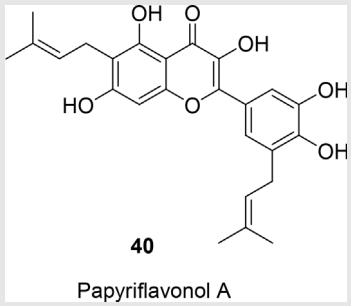

40

Papyriflavonol A

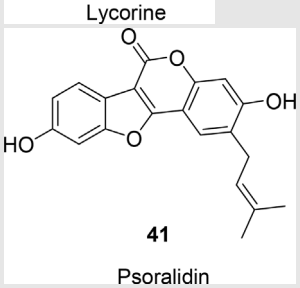

41

Psoralidin

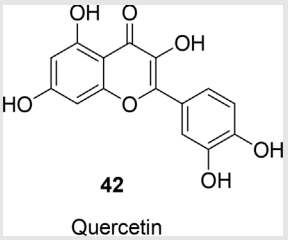

42

Quercetin

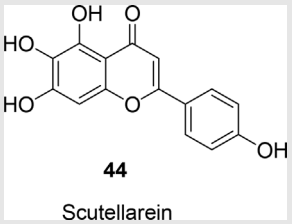

44

Scutellarein

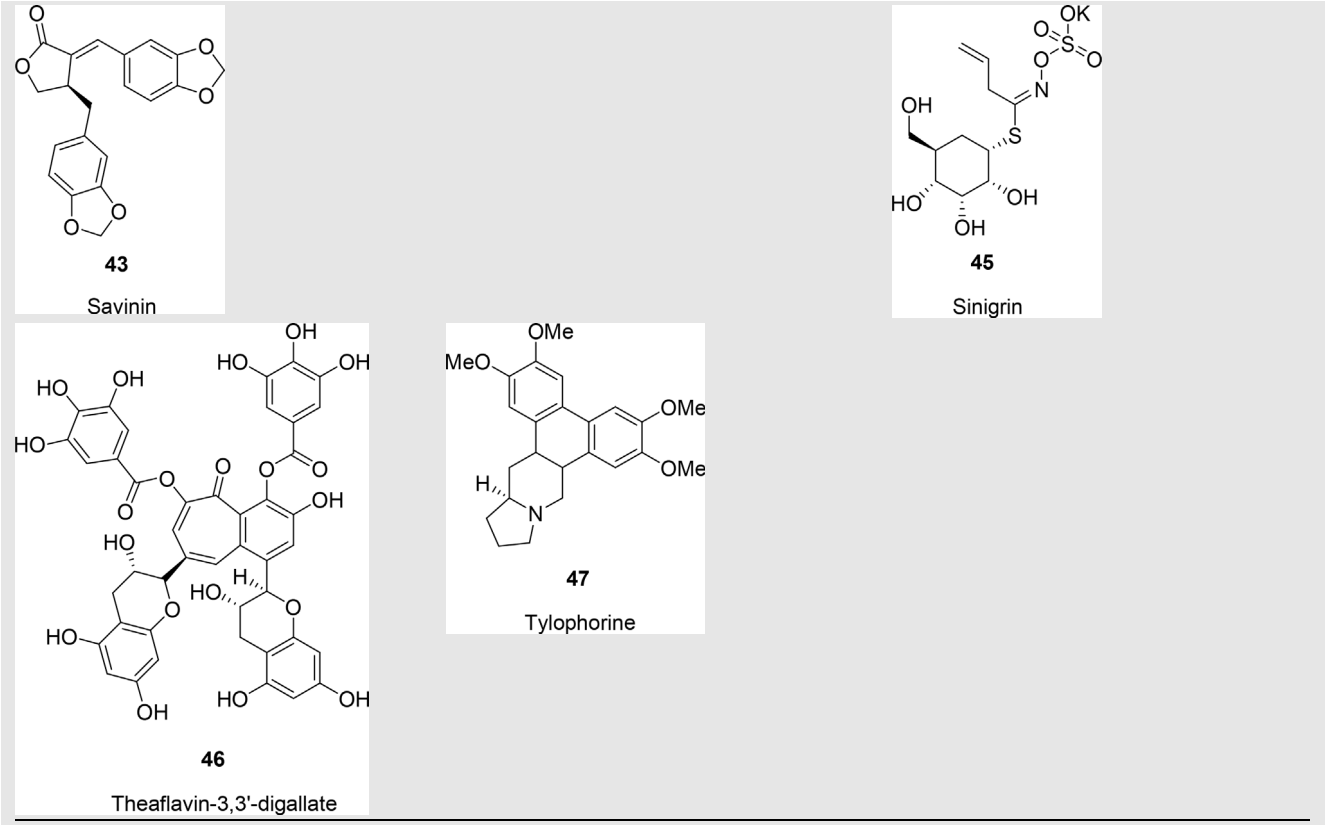

(M^{pro}-X77) and different M^{pro}-phytochemical docked complexes to assess their stability after the phytochemical inhibitor molecule binds to it. The stability was checked using Root Mean Square Deviation (RMSD), Root Mean Square Fluctuation (RMSF), Radius of gyration (Rg) and H-bond interaction analysis [15–17].

The RMSD value is the representation of equilibration of MD trajectories [18–19]. The RMSD values of the protein backbone atoms are usually plotted as a function of time over entire simulation, to analyze the stability of each system. As illustrated from Fig. 8A the RMSD values of control and different M^{pro}-phytochemical inhibitor complexes are determined

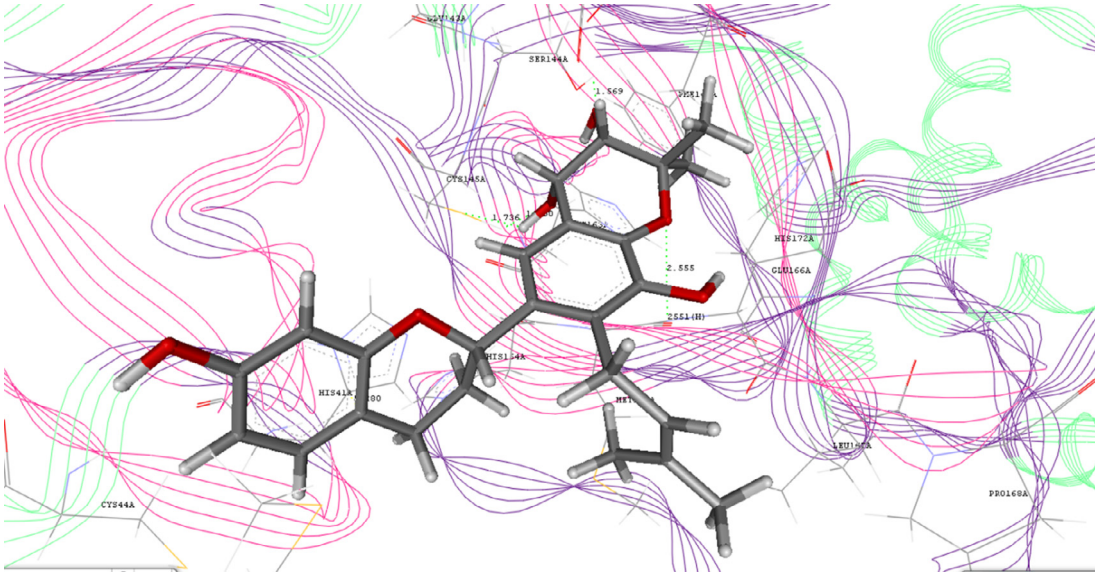

Fig. 1 Docking interaction of **16** (Broussoflavan A).

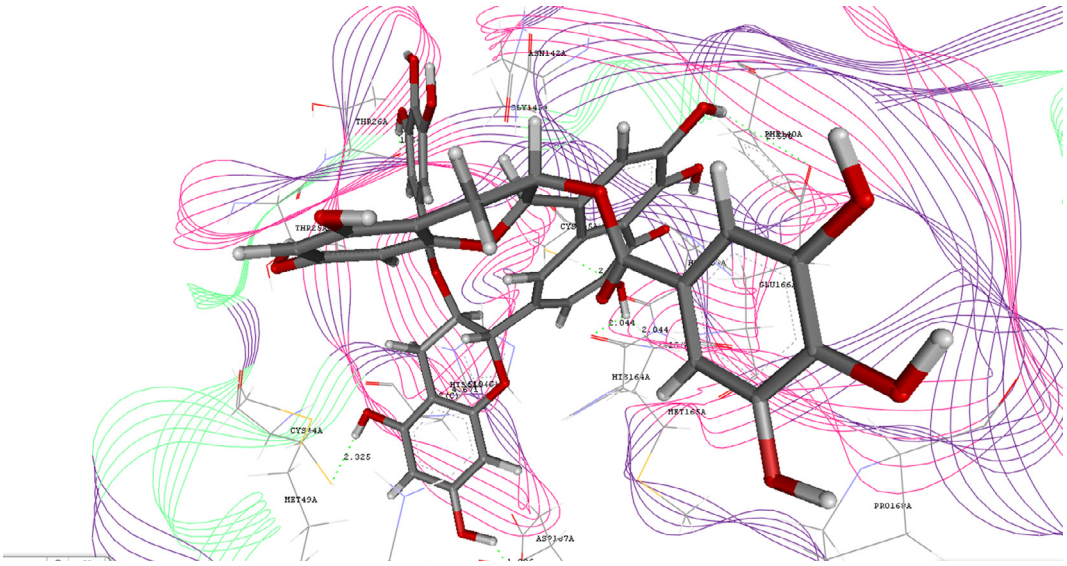

Fig. 2 Docking interaction of **46** (Theaflavin-3,3′-digallate).

over a simulation period of 20 ns. Fig. 8A shows complexes, M^{pro}-**4**, M^{pro}-**16**, M^{pro}-**31** and M^{pro}-**45** have stable RMSD values in the range of 0.1 nm to 0.2 nm with convergence attained after 3 ns simulation period as like control (Fig. 8A). Whereas, complexes M^{pro}-**5**, M^{pro}-**22** and M^{pro}-**46** showed RMSD values in the range of 0.2 nm to 0.3 nm with slight deviation over the range of RMSD values, however with consistency till end of simulation (Fig. 8A). Thus, this is a clear indication of the fact that all phytochemical inhibitors had a stable binding with the SARS-CoV-2 M^{pro} as like control (Fig. 8A).

RMSF value is a marker of flexibility observed of the residues throughout the simulation [18,19]. In present study the flexibility in the residues of SARS-CoV-2 M^{pro} protein was analyzed after binding of different phytochemical inhibitor molecules and compared it with control. In consideration of the average position of the residues, high RMSF value signifies high flexibility, whereas, the low RMSF value indicates lower flexibility throughout the simulation. RMSF values observed for all M^{pro}-phytochemical inhibitor complexes are more or less similar and with significantly lesser fluctuations as like control (Fig. 8B). The active site residues HIS41, SER144, CYS145, HIS163 and GLU166 in all M^{pro}-inhibitor complexes displayed RMSF values of 0.05, 0.07, 0.06, 0.04 and 0.07 nm respectively similar to control (Fig. 8B). Thus, comparison of RMSF value of control and M^{pro}-phytochemical inhibitor docked complexes indicates that the residues bound to phytochemical molecules, **4**, **5**, **16**, **22**, **31**, **45** and **46** are rigid and has limited flexibility in same manner to control (Fig. 8B).

Radius of gyration helps to investigate the changes observed in the conformation of SARS-CoV-2 M^{pro} in terms of compactness after binding of different inhibitor (phytochemical) molecules [18,19]. By meaning, Rg corresponds to

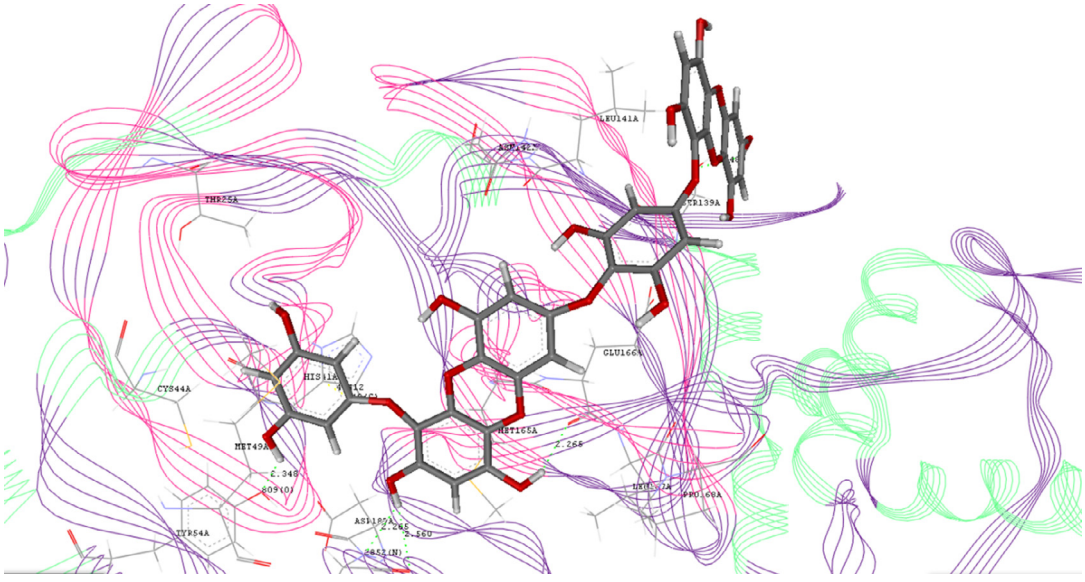

Fig. 3 Docking interaction of **22** (Dieckol).

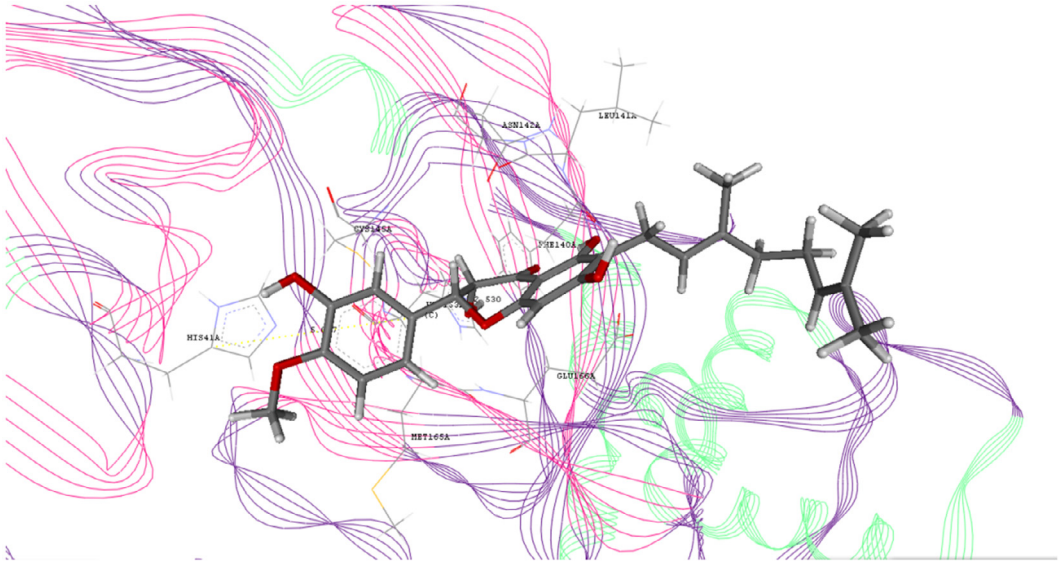

Fig. 4 Docking interaction of **4** (4′-O-Methyldiplacol).

mass weighted root mean square distance of a collection of atoms from their common center of mass. Therefore the overall conformation of the protein could be analyzed by calculating the Rg values. Fig. 8C indicates the Rg values of control and different M^{pro}-inhibitor docked complexes over entire simulation period. The Rg values for control and different M^{pro}-inhibitor complexes were found to be in the range of 2.2 nm to 2.26 nm (Fig. 8C). From this it is apparent that there is no change in the conformation of the M^{pro} protein after binding of different phytochemical inhibitors and also the compactness of M^{pro} structure was found to be similar in presence of experimental inhibitor X77 and computationally identified phytochemical inhibitors (Fig. 8C).

In order to have a stable protein-inhibitor interaction the formation of hydrogen bonds is of supreme importance. For this we have illustrated the number of hydrogen bonds formed between SARS-CoV-2 M^{pro} protein and different phytochemical inhibitor molecules *viz*; **4**, **5**, **16**, **22**, **31**, **45**, **46** and compared it with hydrogen bonding pattern observed in control (Fig. 9**A-H**). Thus, it can be clearly seen from Fig. 9**B-H** that significant hydrogen bonding pattern is observed in all M^{pro}-inhibitor docked complexes in comparison to control (Fig. 9**A**). This is an indication of the fact that there is a strong interaction between SARS-CoV-2 M^{pro} and phytochemical inhibitor molecules *viz;* **4**, **5**, **16**, **22**, **31**, **45**, **46**. As seen from Fig. 9**D-H**, 3 hydrogen bonds are seen in M^{pro}-**16** complex, 4 hydrogen bonds are seen in M^{pro}-**22** complex, 5 hydrogen bonds are observed in M^{pro}-**31** complex, 4 hydrogen bonds are observed in M^{pro}-**45** complex and 6 hydrogen bonds are seen in M^{pro}-**46** complex. Thus, phytochemical inhibitors **16** (Broussoflavan A), **22** (Dieckol), **31** (Hygromycin B), **45** (Sinigrin) and **46** (Theaflavin-3,30-digallate) have

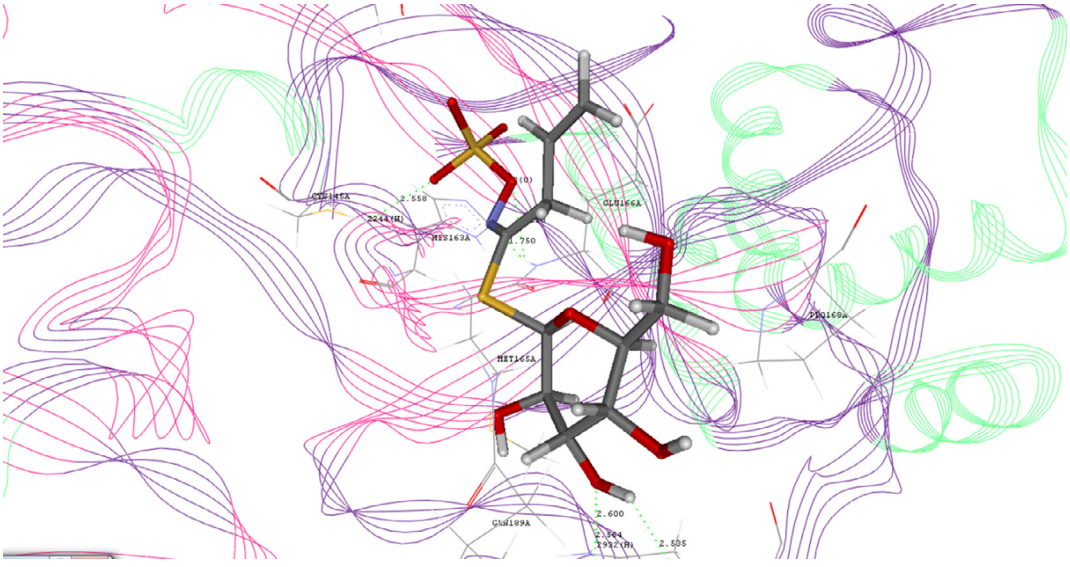

Fig. 5 Docking interaction of **45** (Sinigrin).

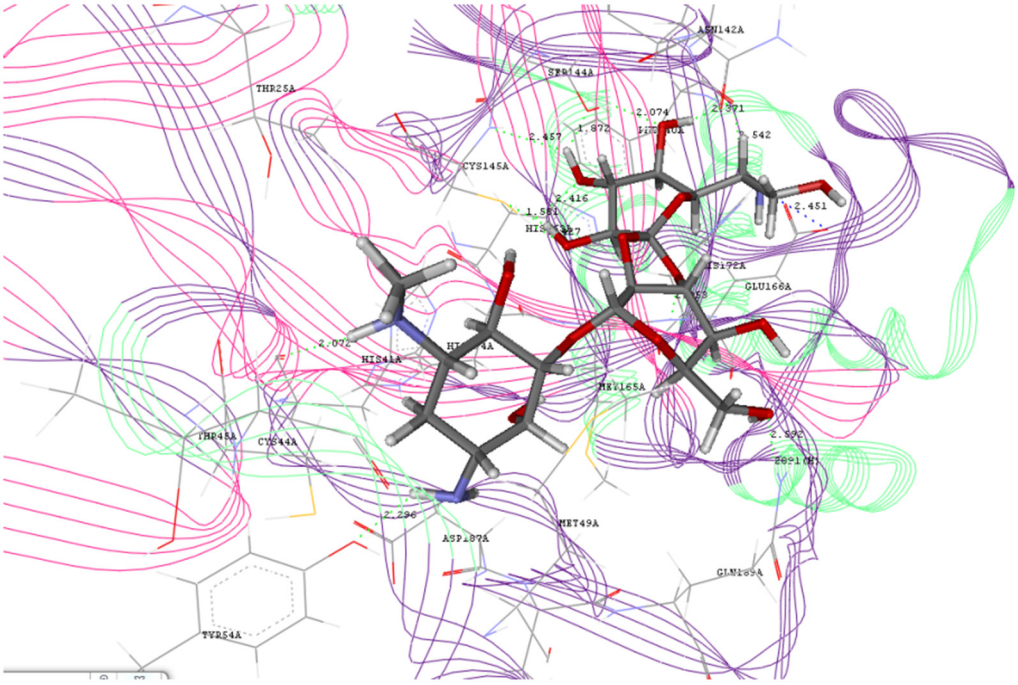

Fig. 6 Docking interaction of **31** (Hygromycin B).

comparatively effective interactions with SARS-CoV-2 M^{pro} as also illustrated from molecular docking study (Table 2).

3. Material and methods

3.1. Preparation of protein structure

The structure of the M^{pro} protein of SARS-CoV-2 (PDB ID: 6W63) [9] was downloaded from the free protein structure database RCSB (www.rcsb.org) with resolution of 2.1 Å. The downloaded protein structure was prepared for the docking analysis using V life MDS 4.6 *via* addition of missing hydrogen atoms. This prepared protein structure was utilized for the docking analysis.

3.2. Preparation of phytochemical structures

The structures of the phytochemical compounds were drawn by using molecule builder module of the V life MDS 4.6 and converted into the 3D structures. These developed structures were then optimized *via* energy minimization using merck molecular force field (MMFF). These optimized structures of phytochemical compounds were utilized for docking analysis.

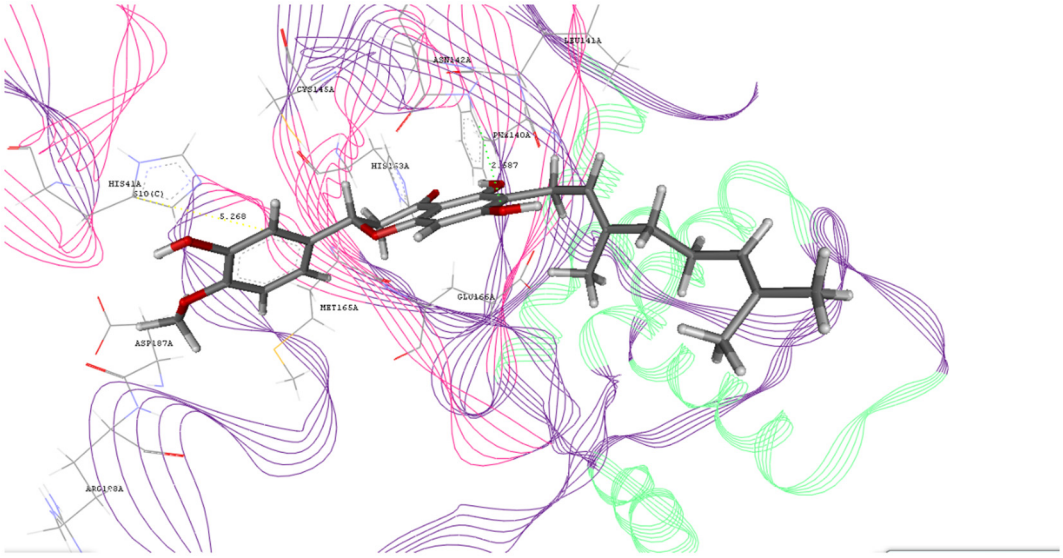

Fig. 7 Docking interaction of **5** (4′-O-Methyldiplacone).

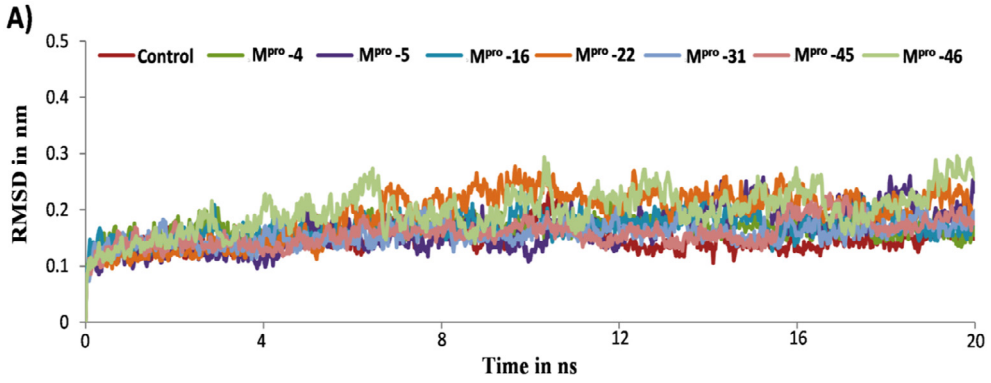

Fig. 8A Molecular dynamics (MD) simulation analysis for most stable docked complexes of SARS-CoV-2 M^{pro} protein with different well-known phytochemicals (inhibitors) in comparison to control. A) Plot of backbone RMSD of SARS-CoV-2 M^{pro}-phytochemical inhibitor complexes along with control during 20 ns simulation.

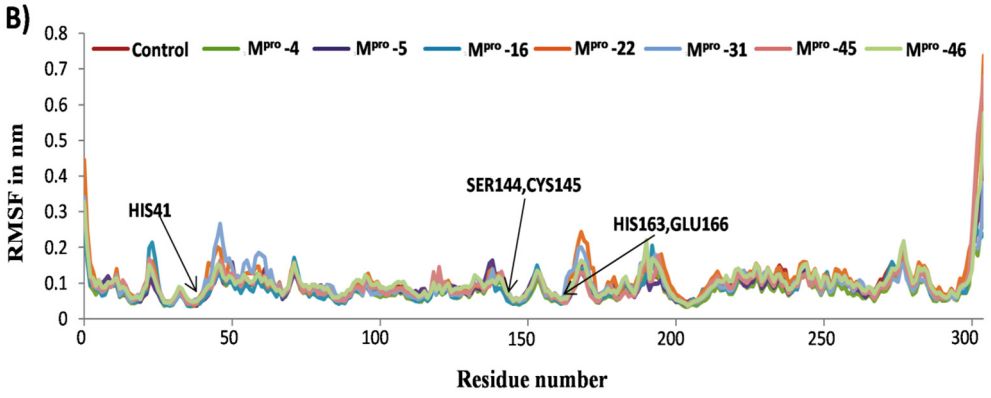

Fig. 8B Molecular dynamics (MD) simulation analysis for most stable docked complexes of SARS-CoV-2 M^{pro} protein with different well-known phytochemicals (inhibitors) in comparison to control. B) RMSF plot of M^{pro}-phytochemical inhibitor complexes along with control during simulation (arrows indicated key active sites of M^{pro} involved in binding with phytochemical inhibitors).

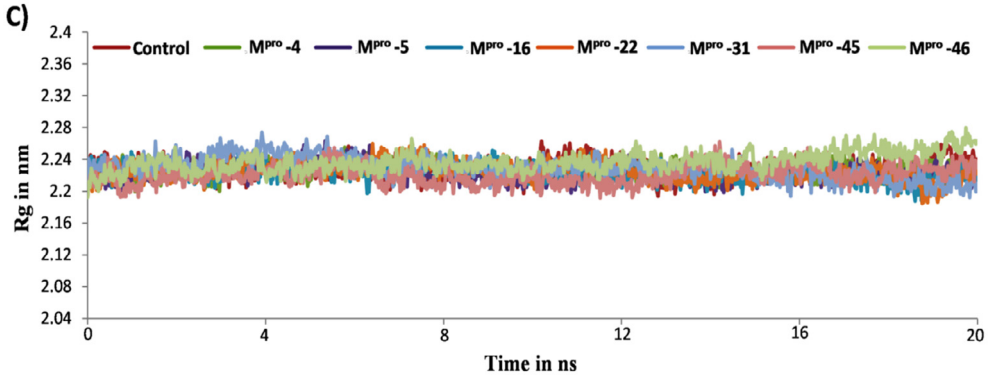

Fig. 8C Molecular dynamics (MD) simulation analysis for most stable docked complexes of SARS-CoV-2 M^{pro} protein with different well-known phytochemicals (inhibitors) in comparison to control. C) Rg plot of SARS-CoV-2 M^{pro}-phytochemical inhibitor complexes along with control during 20 ns simulation representing compactness of receptor M^{pro}.

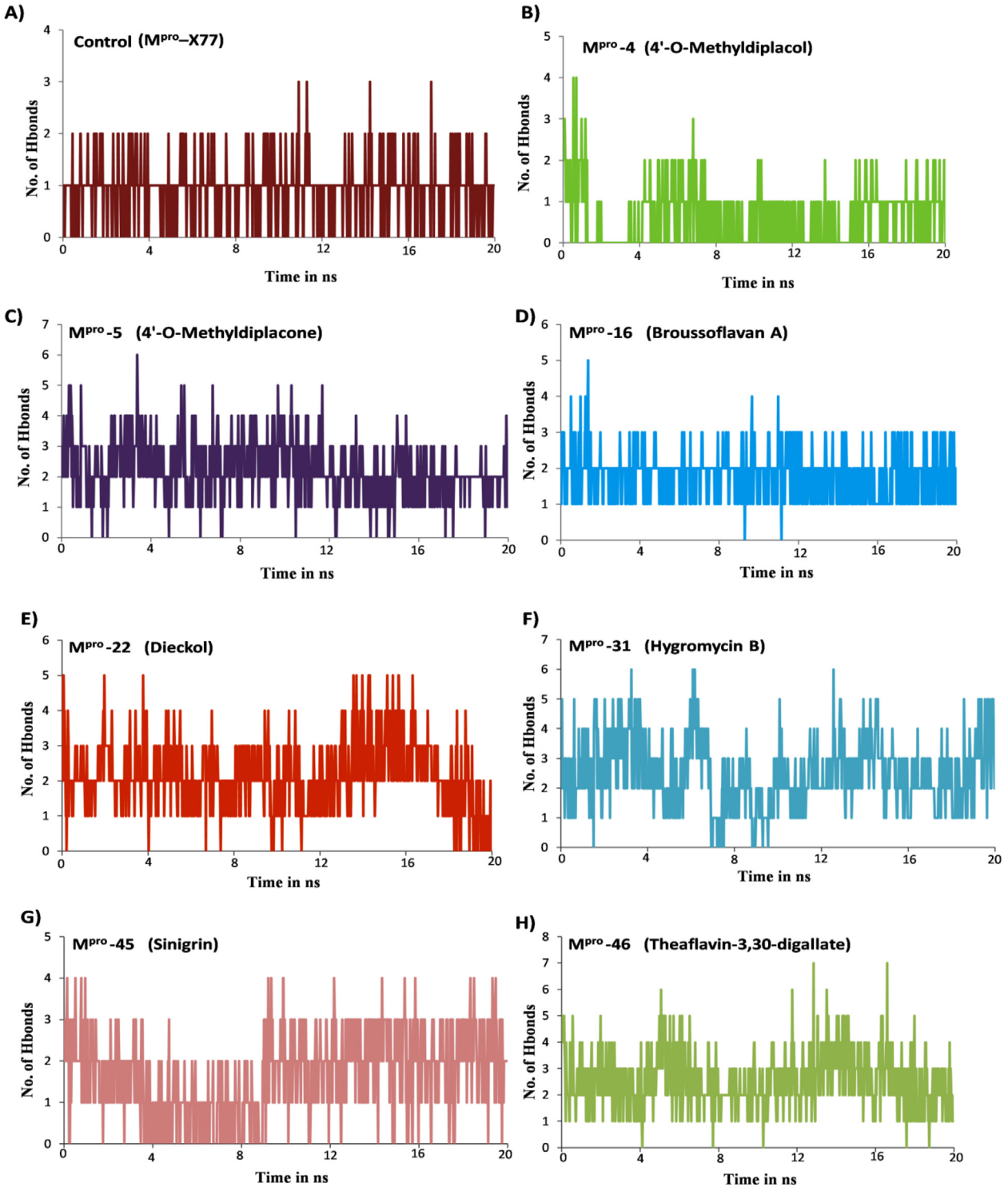

Fig. 9 Hydrogen bond analysis of different SARS-CoV-2 M^{pro}-phytochemical inhibitor complexes in comparison with control for trajectories obtained from 20 ns MD simulations. A) Control (M^{pro}-**X77**). B) M^{pro}-**4** (4′-O-Methyldiplacol). C) M^{pro}-**5**(4′-O-Methyldiplacone). D) M^{pro}-**16** (Broussoflavan A). E) M^{pro}-**22** (Dieckol). F) M^{pro}-**31** (Hygromycin B). G) M^{pro}-**45** (Sinigrin). E) M^{pro}-**46** (Theaflavin-3,30-digallate).

3.3. Molecular docking study

The molecular docking study of the phytochemical compounds with receptor SARS-CoV-2 M^{pro} protein was performed using biopredicta module. Redocking was performed using native ligand X77 of SARS-CoV-2 M^{pro}, to ascertain the docking protocol applied [15–17]. Grip based docking analysis was performed keeping ligand structures in the flexible conformation. For docking analysis the rotational angle was kept at 10° and

Table 2 *In silico* molecular docking interactions of phytochemical compounds with M^{pro} of SARS-CoV-2.

Molecule no.	Name	Interactions				Docking Score
		H bond	Aromatic	Charge	Hydrophobic	
1	3′-O-Methyldiplacol	LEU141(2.3)			MET49, LEU141, ASN142, GLU166	−63.72
2	3′-O-methyldiplacone	LEU141(2.5)			HIS41, LEU141, ASN142, MET165, GLU166, ASP187, ARG188	−63.99
3	4′-O-methylbavachalcone	CYS145 (2.47)			MET165, GLU166	−65.25
4	4′-O-Methyldiplacol	HIS163 (2.5)	HIS41 (5.07)		HIS41, ASN142, MET165, GLU166	−68.78
5	4′-O-Methyldiplacone	ASN142 (2.5)	HIS41 (5.2)		HIS41, LEU141, MET165, GLU166, ASP187, ARG188	−60.58
6	7-Methoxycryptopleurine	SER144 (2.3)	HIS41 (4.6)		THR25, LEU27, HIS41, CYS44, MET49, PHE140, LEU141, ASN142, SER144, CYS145, MET165, GLU166, LUE167, PRO168, GLN189	−56.43
7	Aloe emodin	GLU166 (2.3)	HIS41 (4.4)		ASN142, GLU166	−58.18
8	Amentoflavone	GLU166(1.7) CYS44(2.5)	HIS41 (5.3)			−66.54
9	Apigenin	LEU141 (1.88)	HIS41 (4.2)			−63.17
10	Berbamine		HIS41 (5.4)	HIS163 (3.1)	MET49, PHE140, LEU141, ASN142, GLY143, SER144, CYS145, MET165, GLU166, LEU167, PRO168, GLN189	−30.27
11	Beta-sitosterol	CYS44(1.3)			HIS41, CYS44, MET49, PR52, PRO140, LEU141, ASN142, CYS145, HIS164, MET165, GLU166, ASP187, ARG188, GLN189	−44.75
12	Betulinic acid	GLY143(1.9)		HIS41 (4.7)	THR25, ASN142, MET165, GLU166, LEU167, PRO168	−29.61
13	Betulonic acid	ASN14392.3) GLN189(2.5)			THR25, LEU27, MET49, ASN142, GLY143, CYC145, MET165, GLU166	−35.27
14	Broussochalcone A	HIS163(1.8)	HIS41 (3.7)		MET165, GLU166, ASP187, ARG188, GLN189	−77.70
15	Broussochalcone B	HIS(163(2.2)	HIS41 (4.0), HIS (163 (4.6)		MET165, GLU166, ARG188, GLN189	−68.39
16	Broussoflavan A	SER144(1.5), CYS145(1.6) CYS166(2.5)	HIS41 (1.5)		HIS41, PHE140, LEU141, ASN142, SER144, CYS145, MET165, GLU166, LEU167, PRO168	−91.22
17	Cepharanthine			HIS163 (3.3)	MET49, PHE140, LEU141, ASN142, GLY143, SER144, CYS145, MET165, GLU166, PRO168, GLN189	−24.89
18	Chrysin	GLY143 (1.4), GLU166 (1.99)	HIS41 (4.6)			−54.08
19	Cinanserin	GLY143 (2.2), GLU166(2.4)	HIS41 (4.6), HIS163 (5.4)		MET165, GLU166, LEU167, PRO168, GLN189	−38.67
20	Cinnamtannin B1	HIS41(1.9)	HIS41 (5.01)		HIS41, CYC44, MET49, ASN142, MET165	−59.98
21	Curcumin	PHE140(1.7) THR190(2.1)	HIS163 (4.67)		LEU141, ASN142, MET165, GLU166, LEU167, PRO168, THR190, GLN192	−66.52
22	Dieckol	TYR54(2.3), SER139(2.4), GLU166 (2.2), ARG188 (2.5)	HIS41 (4.4)			−73.11
23	Eckol	CYS145 (2.4), GLU166(2.5)	HIS41 (4.1)			−72.96

(*continued on next page*)

Table 2 (*continued*)

Molecule no.	Name	Interactions				Docking Score
		H bond	Aromatic	Charge	Hydrophobic	
24	Emodin	GLU166(2.2)			CYS145, MET165	−37.28
25	Fangchinoline	GLN 189 (2.4)			HIS41, MET49, HIS164, MET165, PRO168, ASP187, ARG188, GLN189, THR190	−48.40
26	Ferruginol	GLY143(2.3)			HIS41, MET49, PHE140, LEU141, ASN142, MET165, GLU166, GLN 189	−46.19
27	Hesperetin	SER144(1.6) CYS145(2.3) HIS163(2.4)	HIS163 (5.3)		GLU166	−52.42
28	Hexachlorophene	GLU166(2.3)			MET165, GLU166	−59.42
29	Hinokinin	SER144(2.5)			PHE140, LEU141, ASN142, MET165, GLU166, GLN189	−74.70
30	Homoharringtonine	ASN142(2.4)	HIS163 (5.3)		PHE140, LEU141, ASN142, SER144, MET165, GLU166, GLN189	−57.83
31	Hygromycin B	HIS41(2.0), TYR54(2.2), PHE140(2.5) SER144(2.0) CYS145(1.5) GLU166(2.2) GLN189(2.5)		GLU166 (2.4)	THR25, HIS41, CYS44, THR45, MET49, PHE140, LEU141, ASN142, SER144, CYS145, MET165, GLU166, ARG188, GLN189	−62.48
32	Indigo	HIS164(2.2)	HIS41 (4.1)			−74.37
33	Kazinol A	GLU166(2.4)	HIS41		THR25, LEU27, ASN142, GLY143, CYS145, MET165, GLU166, PRO168, ARG188, GLN189	−69.72
34	Kazinol B	GLN189(2.5)			ASN142, MET165, GLN189,	−31.72
35	Kazinol F	CYS145(2.5)			HIS41, MET49, ASN142, GLY143, CYS145, MET165, LEU167, PRO168, ASP187, ARG188, GLN189, GLN192	−58.43
36	Kazinol J	ASN142(2.4)			GLN189, LEU141, ASN142, MET165, GLU166, LEU167, PRO168, GLN189	−63.86
37	Luteolin	ASP187(2.5)	HIS163 (5.3), HIS41 (3.8)			−63.28
38	Lycorine	SER144(2.2)		GLU166 (2.4)	PHE140, LEU141, ASN142, GLU166	−39.07
39	Myricetin	GLU166(2.5)	HIS41 (1.9)			−63.71
40	Papyriflavonol A	GLU166(1.8)			LEU141, MET165, ASP187, ARG188, GLN189	−71.58
41	Psoralidin				MET165, GLU166	−62.19
42	Quercetin	ARG188 (2.5)	HIS41 (4.7)			−64.080
43	Savinin	SER144(2.2)	HIS41 (4.5)		HIS41, LEU141, ASN142, MET165, GLU166, GLN189	−71.08
44	Scutellarein		HIS163 (5.1), HIS41 (4.00)			−64.29
45	Sinigrin	CYS145(2.5) GLU166(2.2) THR190(2.5) GLN192(2.6)			MET165, GLU166, PRO168, GLN189	−65.08
46	Theaflavin-3,3′-digallate	THR26(1.6), CYS44(2.3), CYS145(2.1) HIS164(2.0) MET165 (2.0) GLU166(2.5) ARG188 (1.8)	HIS41 (4.6)		HIS41, MET165	−76.85
47	Tylophorine	CYS145(2.4)		GLU166 (3.4)	LUE141, ASN142, GLY143, SER144, CYS145, MET165, GLN189	−63.57

total number of rotation to 30. The best docking pose of used phytochemical compounds bound to SARS-CoV-2 M^{pro} was selected on the basis of the docking score and type of interactions.

3.4. Molecular dynamics (MD) simulation

Molecular dynamics (MD) simulation was performed to study the dynamic behavior and assess the stability of SARS-CoV-2 M^{pro} protein bound to different phytochemical compounds. The crystal structure of M^{pro} protein of SARS-CoV-2 bound with non-covalent inhibitor X77 (PDB ID: 6 W63) [9] served as a control system in the MD simulation study. The reliability of the binding mode and conformation of predicted best docked phytochemical molecules were confirmed using molecular dynamic simulation of docked complexes by GROMACS 2018.3 (www.gromacs.org) software package [20]. Overall eight M^{pro}-inhibitor complex conformations were considered for MD simulation study, *viz*; a) M^{pro}-**X77** complex which is control, b) M^{pro}-**4** complex consisting phytochemical inhibitor molecule **4′-O-Methyldiplacol**, c) M^{pro}-**5** complex with inhibitor **4′-O-Methyldiplacone**, d) M^{pro}-**16** complex comprising inhibitor **Broussoflavan A**, e) M^{pro}-**22** complex with inhibitor molecule **Dieckol**, f) M^{pro}-**31** complex constituting inhibitor **Hygromycin B**, g) M^{pro}-**45** complex with **Sinigrin** as phytochemical inhibitor molecule and h) M^{pro}-**46** complex having **Theaflavin-3,30-digallate** as inhibitor. The topology of M^{pro} receptor structure was built using pdb2gmx tool incorporating OPLS-AA/L (Optimized Potentials for Liquid-type Simulation) all atom force field [21], whereas topology files of all inhibitor molecules was generated using PRODRG server [22]. After generating topology of each complex, further each complex was centered in the system of cubic box by keeping periodic distance of 1 nm between complex and edge of the box. All complexes were then solvated with SPC216 water molecules to fill the defined box for each complex. The solvated systems were neutralized by addition of suitable number of Na^+ ions to maintain electro-neutrality of the system. The Particle-Mesh-Ewald (PME) method [23] was used for calculation of long-range electrostatic interactions of all the systems. A 50,000-step energy minimization was performed with the steepest descent (SD) method at 300 K by applying periodic boundary conditions (PBC) in all directions. Berendsen thermostat temperature coupling and Parrinello-Rahman pressure coupling for each 500-ps run were used to keep all the systems in equilibrated environment 300 K and 1 bar, respectively. The leap-frog algorithm was used for integrating Newton's equation in molecular dynamics (MD) simulation of all the systems. All the bond lengths were constrained using the LINCS algorithm [24], and the time step was set to 0.002 ps. Finally, a 20-ns MD simulation was carried out for all eight systems. The simulation trajectories obtained after 20 ns MD simulations were analyzed using gmx_rms, gmx_rmsf, gmx_gyrate and gmx_hbond tools from the GROMACS 2018.3 package [20] and visualized using UCSF Chimera molecular visualizing software [25].

4. Conclusion

In the present study, we extensively analyzed the binding potential and mechanism of inhibition of phytochemical towards the SARS-CoV-2 M^{pro} having profound inhibition towards the SARS-CoV-1 M^{pro}. Molecular docking analysis was used to find the number of hydrogen bonds formed between SARS-CoV-2 M^{pro} protein and different inhibitor molecules. Molecular docking analysis along with molecular dynamics simulation analysis showed **16** (Broussoflavan A), **22** (Dieckol), **31** (Hygromycin B), **45** (Sinigrin) and **46** (Theaflavin-3,3′-digallate) have high binding affinity and interaction to the conserved residues of the substrate-binding pocket of SARS-CoV-2 M^{pro}. Thus, these phytochemicals offer preventive and complementary medicine in the fight against viruses due to their natural origin, safety and low cost compared to synthetic drugs. This study provides foundation for the identification of SARS-CoV-2 M^{pro} inhibitors by structural manipulation of active phytochemicals to develop antiviral drugs for future.

CRediT authorship contribution statement

Abdullah G. Al-Sehemi: Conceptualization. **Mehboobali Pannipara:** Writing – original draft. **Rishikesh S. Parulekar:** Software. **Jaydeo T. Kilbile:** Investigation. **Prafulla B. Choudhari:** Writing – review & editing. **Mubarak H. Shaikh:** Review.

Declaration of Competing Interest

The authors declare that they have no known competing financial interests or personal relationships that could have appeared to influence the work reported in this paper.

Acknowledgements

The authors are thankful to the Institute of research and consulting studies at King Khalid University for funding this research through grant number 3-N-20/21. Authors are also thankful to Dr. Yasinalli Tamboli for valuable suggestions during preparation of manuscript.

References

[1] WHO Health Emergency Dashboard WHO (COVID-19) Homepage.
[2] A. Chafekar, B. C. Fielding, MERS-CoV: Understanding the latest human coronavirus threat. *Viruses* 10 (2018) 93-114; 10.3390/v10020093.
[3] J.S.M. Peiris, S.T. Lai, L.L.M. Poon, Y. Guan, L.Y.C. Yam, W. Lim, J. Nicholls, W.K.S. Yee, W.W. Yan, M.T. Cheung, V.C.C. Cheng, K.H. Chan, D.N.C. Tsang, R.W.H. Yung, T.K. Ng, K. Y. Yuen, SARS study group, Coronavirus as a possible cause of severe acute respiratory syndrome, *Lancet* 361 (9366) (2003) 1319–1325.
[4] K. Anand, J. Ziebuhr, P. Wadhwani, J. R. Mesters, R. Hilgenfeld, Coronavirus main proteinase (3CLpro) structure: basis for design of anti-SARS drugs. *Science* 300 (2003) 1763-1767; 10.1126/science.1085658.
[5] (a) P. Zhou, X. L. Yang, X. G. Wang, B. Hu, L. Zhang, W. Zhang, H. R. Si, Y. Zhu, B. Li, C. L. Huang, H. D. Chen, J. Chen, Y. Luo, H. Guo, R. D. Jiang, M. Q. Liu, Y. Chen, X. R. Shen, X. Wang, X. S. Zheng, K. Zhao, Q. J. Chen, F. Deng, L. L. Liu, B. Yan, F. X. Zhan, Y. Y. Wang, G. F. Xiao and Z. L. Shi, A pneumonia outbreak associated with a new coronavirus of probable bat origin. *Nature* 579 (2020) 270-273; 10.1038/s41586-020-2012-7; (b) F. Wu, S. Zhao, B. Yu, Y. M. Chen, W.

Wang, Z. G. Song, Y. Hu, Z. W. Tao, J. H. Tian, Y. Y. Pei, M. L. Yuan, Y. L. Zhang, F. H. Dai, Y. Liu, Q. M. Wang, J. J. Zheng, L. Xu, E. C. Holmes and Y. Z. Zhang, A new coronavirus associated with human respiratory disease in China. *Nature* 579 (2020) 265-269. 10.1038/s41586-020-2008-3.

[6] A. Hegyi, J. Ziebuhr, Conservation of substrate specificities among coronavirus main proteases. J. Gen. Virol. 83 (2002) 595-599; 10.1099/0022-1317-83-3-595.

[7] T. Pillaiyar, M. Manickam, V. Namasivayam, Y. Hayashi and S. H. Jung, An Overview of Severe Acute Respiratory Syndrome-Coronavirus (SARS-CoV) 3CL Protease Inhibitors: Peptidomimetics and Small Molecule Chemotherapy. *J. Med. Chem.* 59 (2016) 6595-6628; 10.1021/acs.jmedchem.5b01461.

[8] Z. Jin, X. Du, Y. Xu, Y. Deng, M. Liu, Y. Zhao, B. Zhang, X. Li, L. Zhang, C. Peng, Y. Duan, J. Yu, L. Wang, K. Yang, F. Liu, R. Jiang, X. Yang, T. You, X. Liu, X. Yang, F. Bai, H. Liu, X. Liu, L.W. Guddat, W. Xu, G. Xiao, C. Qin, Z. Shi, H. Jiang, Z. Rao, H. Yang, Structure of Mpro from SARS-CoV-2 and discovery of its inhibitors, *Nature* 582 (2020) 289–293. https://www.nature.com/articles/s41586-020-2223-y.

[9] A. D. Mesecar, (2020); 10.2210/pdb6w63/pdb.

[10] P.C. Woo, Y. Huang, S.K. Lau, K.Y. Yuen, Coronavirus genomics and bioinformatics analysis, Viruses 2 (2010) 1804–1820.

[11] T. Zhang, Q. Wu, Z. Zhang, Probable pangolin origin of SARS-CoV-2 associated with the COVID-19 outbreak, Curr. Biol. 30 (2020) 1346–1351.e1342.

[12] M. T. Islam, C. Sarkar, D. M. El-Kersh, S. Jamaddar, S. J. Uddin, J. A. Shilpi, M. S. Mubarak, Natural products and their derivatives against coronavirus: A review of the non-clinical and pre-clinical data. *Phytother. Res.* 34 (2020) 2471-2492; 10.1002/ptr.6700.

[13] M. Tahir ul Qamar, S. M. Alqahtani, M. A. Alamri, L. L. Chen, Structural basis of SARS-CoV-2 3CLpro and anti-COVID-19 drug discovery from medicinal plants. J. Pharm. Anal. 10 (2020) 313–319; 10.1016/J.JPHA.2020.03.009.

[14] S. Ben-Shabat, L. Yarmolinsky, D. Porat, A. Dahan, Antiviral effect of phytochemicals from medicinal plants: Applications and drug delivery strategies, Drug. Deliv. Transl. Res. 10 (2020) 354–367; 10.1007/s13346-019-00691-6.

[15] A. G. Al-Sehemi, M. Pannipara, R. S. Parulekar, P. B. Choudhari, M. S. Bhatia, P. K. Zubaidha, Y. Tamboli, Potential of NO donor furoxan as SARS-CoV-2 main protease (M^{pro}) inhibitors: *in silico* analysis, *J. Biol. Struct. Dyn.* 39 (2021) 5804-5818; 10.1080/07391102.2020.1790038.

[16] G. M. Basha, R. S. Parulekar, A. G. Al-Sehemi, M. Pannipara, V. Siddaiah, S. Kumari, P. B. Choudhari, Y. Tamboli, Design and in silico investigation of novel Maraviroc analogues as dual inhibition of CCR-5/SARS-CoV-2 M^{pro}, *J. Biol. Struct. Dyn.* (2021) 1-16; 10.1080/07391102.2021.1955742.

[17] A. G. Al-Sehemi, R. S. Parulekar, M. Pannipara, M. A. PP, P. K. Zubaidha, M. S. Bhatia, T. K. Mohanta and A. Al-Harrasi, *In silico* evaluation of NO donor heterocyclic vasodilators as SARS-CoV-2 M^{pro} protein inhibitor, *J. Biol. Struct. Dyn.* (2021) 1-18; 10.1080/07391102.2021.2005682.

[18] R. S. Parulekar, K. D. Sonawane, Molecular modeling studies to explore the binding affinity of virtually screened inhibitor toward different aminoglycoside kinases from diverse MDR strains, *J. Cell. Biochem.* 119 (2018) 2679-2695; 10.1002/jcb.26435.

[19] R. S. Parulekar and K. D. Sonawane, Insights into the antibiotic resistance and inhibition mechanism of aminoglycoside phosphotransferase from *Bacillus cereus*: In silico and in vitro perspective, *J. Cell. Biochem.* 119 (2018) 9444-9461; 10.1002/jcb.27261.

[20] M. J. Abraham, T. Murtola, R. Schulz, S. Pall, J. C. Smith, B. Hess, E. Lindahl, GROMACS: High performance molecular simulations through multi-level parallelism from laptops to supercomputers, *SoftwareX* 1 (2015) 19-25; 10.1016/j.softx.2015.06.001.

[21] G. A. Kaminski, R. A. Friesner, J. Tirado-Rives, W. L. Jorgensen, Evaluation and reparametrization of the OPLS-AA force field for proteins *via* comparison with accurate quantum chemical calculations on peptides. *J. Phy. Chem. B.* 105 (2001) 6474-6487; 10.1021/jp003919d.

[22] D. M. Van Aalten, R. Bywater, J. B. Findlay, M. Hendlich, R. W. Hooft, G. Vriend, PRODRG, a program for generating molecular topologies and unique molecular descriptors from coordinates of small molecules. *J. Comp. Aided Mol. Des.* 10 (1996) 255-262; 10.1007/BF00355047.

[23] U. Essmann, L. Perera, M.L. Berkowitz, T. Darden, H. Lee, L. G. Pedersen, A smooth particle mesh Ewald method, J. Chem. Phy. 103 (1995) 8577, https://doi.org/10.1063/1.470117.

[24] B. Hess, H. Bekker, H.J. Berendsen, J.G. Fraaije, LINCS: A linear constraint solver for molecular simulations, J. Comp. Chem. 18 (1997) 1463–1472, https://doi.org/10.1002/(SICI)1096-987X(199709)18:12<1463::AID-JCC4>3.0.CO;2-H.

[25] E. F. Pettersen, T. D. Goddard, C. C. Huang, G. S. Couch, D. M. Greenblatt, E. C. Meng, T. E. Ferrin, UCSF chimera-A visualization system for exploratory research and analysis, *J. Comp. Chem.* 25 (2004) 1605-1612; 10.1002/jcc.20084.